Structure of the Chemokine Receptor CXCR1 in Phospholipid Bilayers

Sang Ho Park[1], **Bibhuti B. Das**[1], **Fabio Casagrande**[1], **Ye Tian**[1,2], **Henry J. Nothnagel**[1], **Mignon Chu**[1], **Hans Kiefer**[3], **Klaus Maier**[4], **Anna De Angelis**[4], **Francesca M. Marassi**[2], and **Stanley J. Opella**[1,*]

[1]Department of Chemistry and Biochemistry, University of California, San Diego, 9500 Gilman Drive, La Jolla, California 92093-0307 USA

[2]Sanford-Burnham Medical Research Institute, 10901 North Torrey Pines Road, La Jolla, California 92037 USA

[3]HBC Hochschule Biberach, Karlstrasse 11, 88400 Biberach, Germany

[4]Membrane Receptor Technologies, San Diego, California 92121-3832, USA

Abstract

CXCR1 is one of two high-affinity receptors for the CXC chemokine interleukin-8 (IL-8), a major mediator of immune and inflammatory responses implicated in many disorders, including tumor growth[1-3]. IL-8, released in response to inflammatory stimuli, binds to the extracellular side of CXCR1. The ligand-activated intracellular signaling pathways result in neutrophil migration to the site of inflammation[2]. CXCR1 is a class-A, rhodopsin-like G-protein-coupled receptor (GPCR), the largest class of integral membrane proteins responsible for cellular signal transduction and targeted as drug receptors[4-7]. Despite its importance, its molecular mechanism is poorly understood due to the limited structural information available. Recently, structure determination of GPCRs has advanced by tailoring the receptors with stabilizing mutations, insertion of the protein T4 lysozyme and truncations of their amino acid sequences[8], as well as addition of stabilizing antibodies and small molecules[9] that facilitate crystallization in cubic phase monoolein mixtures[10]. The intracellular loops of GPCRs are critical for G-protein interactions[11] and activation of CXCR1 involves both N-terminal residues and extracellular loops[2,12,13]. Our previous NMR studies indicate that IL-8 binding to the N-terminal residues is mediated by the membrane, underscoring the importance of the phospholipid bilayer for physiological activity[14].

*To whom correspondence should be addressed. sopella@ucsd.edu.

Supplementary information is linked to the online version of the paper at www.nature.com/nature.

Here we report the three-dimensional structure of human CXCR1 determined by NMR spectroscopy. The receptor is in liquid crystalline phospholipid bilayers, without modification of its amino acid sequence and under physiological conditions. Features important for intracellular G-protein activation and signal transduction are revealed.

To examine the structure and function of CXCR1 in its natural environment, we reconstituted the full-length, active receptor in phospholipid bilayers (proteoliposomes). The NMR method we developed, rotationally aligned (RA) solid-state NMR[15], is specifically tailored for the unique properties of membrane proteins in liquid crystalline phospholipid bilayers. It combines features of magic angle spinning (MAS)[16] and oriented sample (OS)[17] solid-state NMR to resolve and assign resonances associated with each amino acid residue, measure site-specific orientation restraints relative to the bilayer, and calculate the three-dimensional structure of the protein and its integral membrane orientation. It differs from previously used OS methods because it relies on the inherent rotational diffusion of membrane proteins in phospholipid bilayers[18] to provide orientation-dependent motional averaging of dipolar coupling (DC) powder patterns relative to the bilayer normal rather than the orientation-dependent frequencies of single-line resonances observed in OS NMR of stationary, uniaxially aligned samples. Furthermore, the method takes advantage of recent bioinformatics developments that facilitate molecular fragment replacement approaches to structure determination, including membrane proteins[19-21].

CXCR1 was uniformly $^{13}C/^{15}N$ labeled by expression in *Escherichia coli*, then purified, refolded in 1,2-dimyristoyl-sn-glycero-3-phosphatidylcholine (DMPC) proteoliposomes[22,23], and placed as a concentrated suspension in a MAS rotor. Refolded CXCR1 binds IL-8 with high affinity (dissociation constant, Kd ~ 1–5 nM) and couples to its G-protein, $G_{i/o}$ (half maximum effective concentration, EC_{50} ~ 1 nM)[22], indicating that the NMR sample conditions are compatible with physiological activity (Supplementary Fig. 1).

As expected, the two-dimensional $^{13}C/^{13}C$ correlation spectrum of this 350-residue protein is quite crowded (Supplementary Fig. 2). However, expansion of the ^{13}CA resonance region has sufficient resolution to contribute to the assignment process (Supplementary Fig. 2d). Spectra, obtained from a uniformly ^{13}C labeled sample with a shorter mixing time and from a sample labeled using 2-^{13}C-glycerol, have fewer signals and improved resolution. Regardless, the vast majority of data used to resolve, assign and measure isotropic chemical shift frequencies from N, CA, CO, and CB sites were obtained from ^{13}C-detected three-dimensional, triple-resonance experiments (Fig. 1b; Supplementary Figs. 3-4; Supplementary Table 2). Overall, 97% of the backbone resonances for residues 20 to 325 were assigned. The missing resonances are from seven Pro (P22, P93, P170, P180, P185, P214, P257) and one Arg (R285). None of the ^{15}N and ^{13}C signals from the mobile N-and C-termini (residues 1-19 and 326-350) could be detected in the spectra, consistent with our observation of these signals in solid-state NMR experiments designed to detect only signals from mobile sites (Supplementary Fig. 6), as well as our previous analysis of local and global motions of CXCR1[24].

Three-dimensional ^{13}C-detected separated local field (SLF) experiments[15] were used to measure the [1]H-^{15}N DC and [1]H-[13]CA DC frequencies that provide orientation restraints for structure determination (Fig. 1c, 1d; Supplementary Fig. 5). The protein backbone structure was calculated by a molecular fragment replacement approach. An initial structural model was generated from a set of molecular fragments generated with CS-Rosetta[20] from the experimental chemical shifts, the amino acid sequence of CXCR1, and the helical framework of the prototypical class A GPCR bovine rhodopsin[25]. This initial model was first refined with the experimental restraints using the all atom[19] and the implicit membrane[21] potentials of Rosetta. Finally, the resulting structural model was refined by restrained simulated annealing using Xplor-NIH[26].

The three-dimensional structure of CXCR1 (Fig. 1e) has the consensus fold of a GPCR, with seven transmembrane helices (TM1-TM7) connected by three extracellular loops (ECL1-ECL3) and three intracellular loops (ICL1-ICL3). The average backbone pairwise RMSD is 1.7 Å (Supplementary Table 1) and the experimentally measured [1]H-^{15}N DC and [1]H-[13]CA DC values correlate remarkably well with those calculated from the refined protein structure (Fig. 1g; Supplementary Fig. 7). Notably, the correlations improve dramatically following refinement of the initial structural model with the experimental data, demonstrating that the NMR structure of CXCR1 is determined by the experimentally measured backbone orientation restraints and dihedral angles. We anticipate that both structural accuracy and precision will improve with inclusion of side chain restraints and, where feasible, distance restraints.

DCs contain information about molecular orientation as well as dynamics, and scaling of their values by local internal motions would compromise their analysis in terms of pure orientation restraints. For CXCR1, analysis of the DC data yielded similar values of the magnitude and symmetry of the molecular order tensor for residues in the helices and loops, indicating that these regions of the protein experience a similar degree of order in the lipid bilayer. This is supported by the excellent fit of the DC correlation plots obtained with a single value of the order tensor (Fig. 1g; Supplementary Fig. 7b) and by the observation that >20% of the [1]H-^{15}N DC signals from residues distributed throughout the protein sequence, including in loop sites, fall within 10% of the maximum value (21 kHz) expected for a static crystalline sample (Fig. 1d).

Following the structure determination of rhodopsin from three- and two-dimensional crystals[25,27], the structures of several class A ligand-activated GPCRs have recently been determined by X-ray crystallography[6,7]. CXCR1 is now the first GPCR with its structure determined in liquid crystalline phospholipid bilayers, and the first ligand-activated GPCR with its structure determined without modification of its amino acid sequence. The structure of CXCR1 shares significant similarities with that of CXCR4[28], the only other chemokine receptor whose structure has been determined (Fig. 3; Supplementary Fig. 8). However, there are some notable differences reflecting the modifications made to the sequence of CXCR4 required for crystallization (insertion of T4 lysozyme in ICL3, removal of 33 C-terminal residues and L125W mutation), the amino acid sequence differences between the two proteins, the influence of the planar phospholipid bilayer, or the rotational diffusion of the protein.

The CXCR1 helices are well defined by the spectroscopic data. For example, a plot of the measured values of the amide ^{1}H-^{15}N DC versus residue number yields a characteristic wave-like pattern[29] reflecting helical structure (Fig. 1d), with breaks in the waves corresponding to helix termini or kinks. For example, the DC data show the presence of a kink that changes the direction of helix TM2 (residues 74-101) at Phe88, coinciding with a kink at the same location in CXCR4 (Fig. 3). The extracellular start of TM7, just following ECL3, is tilted towards the receptor's central axis in CXCR1, although it is less well defined in CXCR1 than in CXCR4 where residues in the N-terminus of TM7 interact with the added compound IT1t[28]. Helix TM7 is also about one turn longer at the intracellular end than its counterpart in CXCR4, extending to Ile308, three residues beyond the conserved GPCR sequence NPxxY. Furthermore, residues immediately preceding the mobile C terminus of CXCR1 form a well-defined helix (H8; residues Gln310 to Ala321) that is absent in the structure of CXCR4 (Fig. 2, 3; Supplementary Fig. 8). H8 has a distinctly amphipathic amino acid sequence and aligns along the membrane surface, indicating that the phospholipid bilayer may play a role in stabilizing its conformation.

The NMR data further reveal the presence of two disulfide bonds (Fig. 2b; Supplementary Fig. 9) that are also present in CXCR4, one connecting the N-terminus to the extracellular start of TM7 (Cys30-Cys277) and the other connecting the extracellular end of TM3 to ECL2 (Cys110-Cys187). These Cys pairs are highly conserved in the sequences of chemokine receptors and are important for ligand binding. Together, they play a significant role in shaping the extracellular structure of the receptor, and also provide useful restraints for structure determination. The long ECL2 of CXCR1 forms a β-hairpin whose structure is constrained by the Cys110-Cys187 disulfide bond. A similar structure is observed in CXCR4 and in many other GPCRs, despite a lack of amino acid sequence similarity in this region. However, the ECL2 β-hairpin of CXCR1 is less well defined than that of CXCR4, consistent with the presence of two Pro residues in CXCR1.

In both CXCR1 and CXCR4, charged residues are mainly located near the membrane-water interface (Supplementary Fig. 10), with negative charges clustered in the extracellular loops where they can play a role in ligand binding and receptor activation. In addition, four charged residues, contributed by helices TM2 (Asp85), TM3 (Lys117) and TM7 (Asp288, Glu291), form a polar cluster in the core of the helical bundle of CXCR1 that may have important consequences for ligand binding and receptor signal transduction. One of these residues (Asp288) is not conserved in CXCR4 and may contribute to the differences in biological activities of the two chemokine receptors.

The intracellular loops of GPCRs are critical for G-protein interactions[11]. Modification of ICL3 by insertion of T4 lysozyme between TM5 and TM6, rendered CXCR4 incapable of activating G-proteins[28]. In contrast, unmodified CXCR1 is fully active with respect to both G-protein activation and chemokine binding, and its three intracellular loops are structurally well defined (Fig. 2, Fig. 3c, Supplementary Fig. 8). Notably, ICL3, which is important for CXCR1 coupling to G-proteins and involved in calcium mobilization, chemokine-mediated migration, and cell adhesion, extends from Thr228 to Gln236, connecting helices TM5 and TM6, which are both one turn shorter than the corresponding helices in CXCR4. ICL3 protrudes into the cytoplasm where it is available for G-protein binding. Its sequence shares

significant homology with other GPCRs; therefore, the ability to observe the structure of an intact GPCR provides an opportunity to propose structure-based mechanisms of G-protein binding and activation.

CXCR1 has been the subject of significant molecular modeling efforts aimed at understanding its interactions with small molecule inhibitors, including compounds active in reducing breast cancer metastasis[30]. The structure of CXCR1 determined in a lipid bilayer membrane should facilitate these studies. The solid-state NMR approach used for structure determination has several significant advantages. The protein resides in fully hydrated liquid crystalline phospholipid bilayers at physiological conditions of temperature and pH, and no detergents or non-native lipid phases are present. The protein sequence is unmodified, with no truncations, mutations, or insertions of foreign proteins. The phospholipid composition can be varied, and other components, such as cholesterol, can be added. Other proteins or small molecules, including chemokines, G-proteins, nanobodies, and drugs can be added directly to the samples, enabling detection of any structural changes by direct spectroscopic and structural comparisons. NMR is adept at describing both overall and local protein dynamics. Measurements of DCs and isotropic chemical shifts to provide molecular orientation and dihedral angle restraints, combined with refinement in a membrane environment, facilitate structure determination by molecular fragment replacement. These can be supplemented with orientation restraints derived from rotationally averaged chemical shift anisotropy powder patterns to further improve structural accuracy and precision. Thus, we anticipate that this method will enable structure determination and structure-activity studies of other GPCRs as well as a wide range of other membrane proteins under near-native conditions.

METHODS

Sample Preparation

Full-length human CXCR1 (residues 1 to 350) was expressed with an N-terminal GST partner and a C-terminal His_6 tag in *E. coli* BL21 cells. Isotopically labeled samples were obtained by growing bacteria in M9 media containing ^{15}N labeled ammonium sulfate and $^{13}C_6$-glucose or 2-^{13}C-glycerol (Cambridge Isotope Laboratories). A sample of selectively $^{13}C/^{15}N$-Phe labeled CXCR1 was also prepared. After cell lysis, the GST-CXCR1-His_6 fusion protein was bound to Ni-NTA resin. CXCR1 was separated from GST by incubation with thrombin and then purified and refolded in DMPC proteoliposomes by detergent dialysis[22,23,31]. The resulting proteoliposomes were suspended in buffer, isolated by ultra-centrifugation, and packed as a hydrated pellet into the MAS rotor. Detailed sample preparation methods are provided in Supplementary Information.

Ligand binding and G-protein activation

To assay IL-8 ligand binding, CXCR1 proteoliposomes were incubated with varying concentrations of ^{125}I-labeled and unlabeled IL-8, and bound IL-8 was determined by measuring radioactivity in a scintillation counter after removing any free IL-8 ligand (Supplementary Fig. 1a)[22,31]. To assay G-protein activation, CXCR1 proteoliposomes were reconstituted with $G_{i/o}$ protein trimer, and used to measure ^{35}S-GTPγS binding as a function

of agonist IL-8 concentration (Supplementary Fig. 1b)[22,31]. Refolded CXCR1 binds IL-8 (Kd ~ 1–5 nM) and activates G-protein in a ligand-dependent manner (EC$_{50}$ ~ 1 nM), with affinities similar to those reported in the literature[1,32].

NMR Spectroscopy

NMR experiments, experimental parameters and measurements of restraints are described in Supplementary Information, including Supplementary Table 2. ^{13}C chemical shifts were externally referenced to DSS by setting the adamantane methylene carbons to a ^{13}C chemical shift frequency of 40.48 ppm; ^{15}N chemical shifts were externally referenced to liquid ammonia by setting the ammonium sulfate nitrogen to 26.8 ppm[33,34]. Fast rotational diffusion (>10^5 Hz) of the protein was verified by analysis of ^{13}CO powder pattern line shapes[35]. Sample integrity was ascertained by monitoring one- and two-dimensional spectra.

Resonances from residues 20-325 of CXCR1 were all assigned, except for those corresponding to seven Pro residues (P22, P93, P170, P180, P185, P214 and P257) and one Arg (R285). Two disulfide bonds (C30-C277, C110-C187) were determined from the characteristic CB and CA chemical shifts that reflect the oxidation states of Cys sites[36]. Backbone dihedral angle (φ, ψ) restraints were derived from the experimentally measured isotropic chemical shifts using CS-Rosetta[20] and TALOS[37,38]. Values of the experimental ^{1}H-^{15}N DC and ^{1}H-^{13}CA DC used in the structure calculations were measured from the perpendicular edge frequencies of the respective rotationally averaged powder patterns. For each DC, the perpendicular edge frequency was multiplied by 4 to obtain the frequency of dipolar splitting between the parallel edges of the Pake doublet. In most measurements, the sign of the ^{1}H-^{15}N DC could be determined unambiguously[39]. In cases where this was not possible, and for all of the ^{1}H-^{13}CA DC data, the DC restraints were implemented as absolute values in the structure calculations.

Structure Calculations

Structure calculations were performed in three stages using the programs: CS-Rosetta[20]; Rosetta[19,21] (including both the coarse-grained and all-atom potentials[19] as well as the implicit membrane potential[21] available in Rosetta version 3.2); and Xplor-NIH[26].

In the first stage, we used CS-Rosetta together with the amino acid sequence of CXCR1 and the assigned isotropic chemical shifts from CA, CB, CO, and N protein sites, to generate a molecular fragment database, containing 67,784 9-residue fragments and 69,204 3-residue fragments.

In the second stage, we used the resulting molecular fragment database, together with the experimental DC restraints and the structure of rhodopsin (PDB ID: 1F88)[25] as topology template, to fold 20,000 structural models with the coarse-grained and implicit membrane potentials of Rosetta. These coarse-grained structural models were evaluated according to their Rosetta energy and backbone CA RMSD to the lowest energy structure. The 1,000 lowest energy models were selected for further refinement using the all-atom energy function and implicit membrane environment of Rosetta, together with the experimental DC restraints, and the experimentally determined disulfide bond restraints. The Rosetta all-atom relax protocol was implemented for 10 cycles with an increasing ^{1}H-^{15}N DC restraint

weighting factor ramped from 1 to 3 kcal•mol^{-1}•Hz^{-2}. The lowest energy structure was selected for further refinement in the next stage. Convergence of the Rosetta calculations is shown in Supplementary Fig. 11.

In the third and final stage, structure refinement was performed using a simulated annealing protocol with Xplor-NIH internal variable molecular dynamics[40] and all the experimental NMR restraints. During simulated annealing, the temperature was lowered from 500 K to 50 K. Experimentally determined disulfide bonds were included by explicit definition in the molecular structure file of CXCR1. Backbone dihedral angles were imposed with a range of ±2° for helices and ±30° for loops, and a fixed force constant (1,000 kcal•mol^{-1}•rad^{-2}). ^{1}H-^{15}N DC restraints were imposed with a range of ±2 kHz and a ramped force constant (0.1-2.5 kcal•mol^{-1}•kHz^{-2}). ^{1}H-^{13}CA DC restraints were imposed with a range of ±4 kHz and a ramped force constant (0.05-1.25 kcal•mol^{-1}•kHz^{-2}). The protocol also included a potential for knowledge-based torsion angles[41] implemented with a dimensionless force constant (0.2), a potential for the radius of gyration[42] implemented for residues 28 to 325 with a fixed force constant (10 kcal•mol^{-1}•Å^{-2}), plus energy terms to enforce covalent geometry and prevent atomic overlap[43].

The magnitude and symmetry of the molecular alignment tensor were fixed, with values of the axial alignment (Da) and rhombicity (Rh) parameters set to 10.52 kHz and 0, respectively, as expected for a membrane protein in phospholipid bilayers with an order parameter of 1.0 and an amide NH bond length of 1.05 Å. The ^{1}H-^{13}CA DC alignment tensor was normalized to the maximum value of the ^{1}H-^{15}N DC.

A total of 100 structures were calculated and the 10 lowest energy structures were selected as the structural ensemble for analysis (Fig. 1e, Supplementary Table 1). Ramachandran Plot Statistics were evaluated with the program PROCHECK[44]. Molecular structures were analyzed and visualized with Pymol[45]. RMSDs and R factors, reflecting correlations between experimentally observed values of the restraints and values calculated from the refined structure, were estimated as described[46].

Supplementary Material

Refer to Web version on PubMed Central for supplementary material.

Acknowledgments

References

1. Holmes WE, Lee J, Kuang WJ, Rice GC, Wood WI. Structure and functional expression of a human interleukin-8 receptor. Science. 1991; 253:1278–1280. [PubMed: 1840701]

2. Sallusto F, Baggiolini M. Chemokines and leukocyte traffic. Nat Immunol. 2008; 9:949–952. [PubMed: 18711431]

3. Waugh DJ, Wilson C. The interleukin-8 pathway in cancer. Clin Cancer Res. 2008; 14:6735–6741. [PubMed: 18980965]

4. Rajagopal S, Rajagopal K, Lefkowitz RJ. Teaching old receptors new tricks: biasing seven-transmembrane receptors. Nat Rev Drug Discov. 2010; 9:373–386. [PubMed: 20431569]

5. Goncalves JA, Ahuja S, Erfani S, Eilers M, Smith SO. Structure and function of G protein-coupled receptors using NMR spectroscopy. Prog Nucl Magn Reson Spectrosc. 2010; 57:159–180. [PubMed: 20633362]

6. Rosenbaum DM, Rasmussen SG, Kobilka BK. The structure and function of G-protein-coupled receptors. Nature. 2009; 459:356–363. [PubMed: 19458711]

7. Katritch V, Cherezov V, Stevens RC. Diversity and modularity of G protein-coupled receptor structures. Trends Pharmacol Sci. 2012; 33:17–27. [PubMed: 22032986]

8. Rosenbaum DM, et al. GPCR engineering yields high-resolution structural insights into beta2-adrenergic receptor function. Science. 2007; 318:1266–1273. [PubMed: 17962519]

9. Rasmussen SG, et al. Crystal structure of the human beta2 adrenergic G-protein-coupled receptor. Nature. 2007; 450:383–387. [PubMed: 17952055]

10. Landau EM, Rosenbusch JP. Lipidic cubic phases: a novel concept for the crystallization of membrane proteins. Proc Natl Acad Sci U S A. 1996; 93:14532–14535. [PubMed: 8962086]

11. Oldham WM, Hamm HE. Heterotrimeric G protein activation by G-protein-coupled receptors. Nature reviews. 2008; 9:60–71.

12. Crump MP, et al. Solution structure and basis for functional activity of stromal cell-derived factor-1; dissociation of CXCR4 activation from binding and inhibition of HIV-1. EMBO J. 1997; 16:6996–7007. [PubMed: 9384579]

13. Rajagopalan L, Rajarathnam K. Ligand selectivity and affinity of chemokine receptor CXCR1. Role of N-terminal domain. J Biol Chem. 2004; 279:30000–30008. [PubMed: 15133028]

14. Park SH, Casagrande F, Cho L, Albrecht L, Opella SJ. Interactions of interleukin-8 with the human chemokine receptor CXCR1 in phospholipid bilayers by NMR spectroscopy. J Mol Biol. 2011; 414:194–203. [PubMed: 22019593]

15. Das BB, et al. Structure Determination of a Membrane Protein in Proteoliposomes. J Am Chem Soc. 2012; 134:2047–2056. [PubMed: 22217388]

16. McDermott A. Structure and dynamics of membrane proteins by magic angle spinning solid-state NMR. Annu Rev Biophys. 2009; 38:385–403. [PubMed: 19245337]

17. Opella SJ, Marassi FM. Structure determination of membrane proteins by NMR spectroscopy. Chem Rev. 2004; 104:3587–3606. [PubMed: 15303829]

18. Edidin M. Rotational and translational diffusion in membranes. Annu Rev Biophys Bioeng. 1974; 3:179–201. [PubMed: 4371655]

19. Das R, Baker D. Macromolecular modeling with rosetta. Annu Rev Biochem. 2008; 77:363–382. [PubMed: 18410248]

20. Shen Y, et al. Consistent blind protein structure generation from NMR chemical shift data. Proc Natl Acad Sci U S A. 2008; 105:4685–4690. [PubMed: 18326625]

21. Yarov-Yarovoy V, Schonbrun J, Baker D. Multipass membrane protein structure prediction using Rosetta. Proteins. 2006; 62:1010–1025. [PubMed: 16372357]

22. Park SH, et al. High-resolution NMR spectroscopy of a GPCR in aligned bicelles. J Am Chem Soc. 2006; 128:7402–7403. [PubMed: 16756269]

23. Park SH, et al. Optimization of purification and refolding of the human chemokine receptor CXCR1 improves the stability of proteoliposomes for structure determination. Biochim Biophys Acta. 2012; 1818:584–591. [PubMed: 22024025]

24. Park SH, et al. Local and global dynamics of the G protein-coupled receptor CXCR1. Biochemistry. 2011; 50:2371–2380. [PubMed: 21323370]

25. Palczewski K, et al. Crystal structure of rhodopsin: A G protein-coupled receptor. Science. 2000; 289:739–745. [PubMed: 10926528]

26. Schwieters CD, Kuszewski JJ, Tjandra N, Clore GM. The Xplor-NIH NMR molecular structure determination package. J Magn Reson. 2003; 160:65–73. [PubMed: 12565051]

27. Krebs A, Edwards PC, Villa C, Li J, Schertler GF. The three-dimensional structure of bovine rhodopsin determined by electron cryomicroscopy. J Biol Chem. 2003; 278:50217–50225. [PubMed: 14514682]

28. Wu B, et al. Structures of the CXCR4 chemokine GPCR with small-molecule and cyclic peptide antagonists. Science. 2010; 330:1066–1071. [PubMed: 20929726]

29. Mesleh MF, et al. Dipolar waves map the structure and topology of helices in membrane proteins. J Am Chem Soc. 2003; 125:8928–8935. [PubMed: 12862490]

30. Ginestier C, et al. CXCR1 blockade selectively targets human breast cancer stem cells in vitro and in xenografts. J Clin Invest. 2010; 120:485–497. [PubMed: 20051626]

31. Casagrande, F.; Maier, K.; Kiefer, H.; Opella, SJ.; Park, SH. Production of Membrane Proteins. Wiley-VCH Verlag GmbH & Co. KGaA; 2011. p. 297-316.

32. Murphy PM, Tiffany HL. Cloning of complementary DNA encoding a functional human interleukin-8 receptor. Science. 1991; 253:1280–1283. [PubMed: 1891716]

33. Wishart DS, et al. 1H, 13C and 15N chemical shift referencing in biomolecular NMR. J Biomol NMR. 1995; 6:135–140. [PubMed: 8589602]

34. Morcombe CR, Zilm KW. Chemical shift referencing in MAS solid state NMR. J Magn Reson. 2003; 162:479–486. [PubMed: 12810033]

35. Park SH, Das BB, De Angelis AA, Scrima M, Opella SJ. Mechanically, magnetically, and "rotationally aligned" membrane proteins in phospholipid bilayers give equivalent angular constraints for NMR structure determination. J Phys Chem B. 2010; 114:13995–14003. [PubMed: 20961141]

36. Sharma D, Rajarathnam K. 13C NMR chemical shifts can predict disulfide bond formation. J Biomol NMR. 2000; 18:165–171. [PubMed: 11101221]

37. Cornilescu G, Delaglio F, Bax A. Protein backbone angle restraints from searching a database for chemical shift and sequence homology. J Biomol NMR. 1999; 13:289–302. [PubMed: 10212987]

38. Shen Y, Delaglio F, Cornilescu G, Bax A. TALOS+: a hybrid method for predicting protein backbone torsion angles from NMR chemical shifts. J Biomol NMR. 2009; 44:213–223. [PubMed: 19548092]

39. Denny JK, Wang J, Cross TA, Quine JR. PISEMA powder patterns and PISA wheels. J Magn Reson. 2001; 152:217–226. [PubMed: 11567575]

40. Schwieters CD, Clore GM. Internal coordinates for molecular dynamics and minimization in structure determination and refinement. J Magn Reson. 2001; 152:288–302. [PubMed: 11567582]

41. Kuszewski J, Gronenborn AM, Clore GM. Improvements and extensions in the conformational database potential for the refinement of NMR and X-ray structures of proteins and nucleic acids. J Magn Reson. 1997; 125:171–177. [PubMed: 9245376]

42. Kuszewski J, Gronenborn AM, Clore GM. Improving the Packing and Accuracy of NMR Structures with a Pseudopotential for the Radius of Gyration. J Am Chem Soc. 1999; 121:2337–2338.

43. Nilges M, Clore GM, Gronenborn AM. Determination of three-dimensional structures of proteins from interproton distance data by dynamical simulated annealing from a random array of atoms. Circumventing problems associated with folding. FEBS Lett. 1988; 239:129–136. [PubMed: 3181419]

44. Laskowski RA, Rullmannn JA, MacArthur MW, Kaptein R, Thornton JM. AQUA and PROCHECK-NMR: programs for checking the quality of protein structures solved by NMR. J Biomol NMR. 1996; 8:477–486. [PubMed: 9008363]

45. DeLano, WL. PyMol. 2005. www.pymol.org

46. Clore GM, Garrett DS. R-factor, Free R, and Complete Cross-Validation for Dipolar Coupling Refinement of NMR Structures. J Am Chem Soc. 1999; 121:9008–9012.
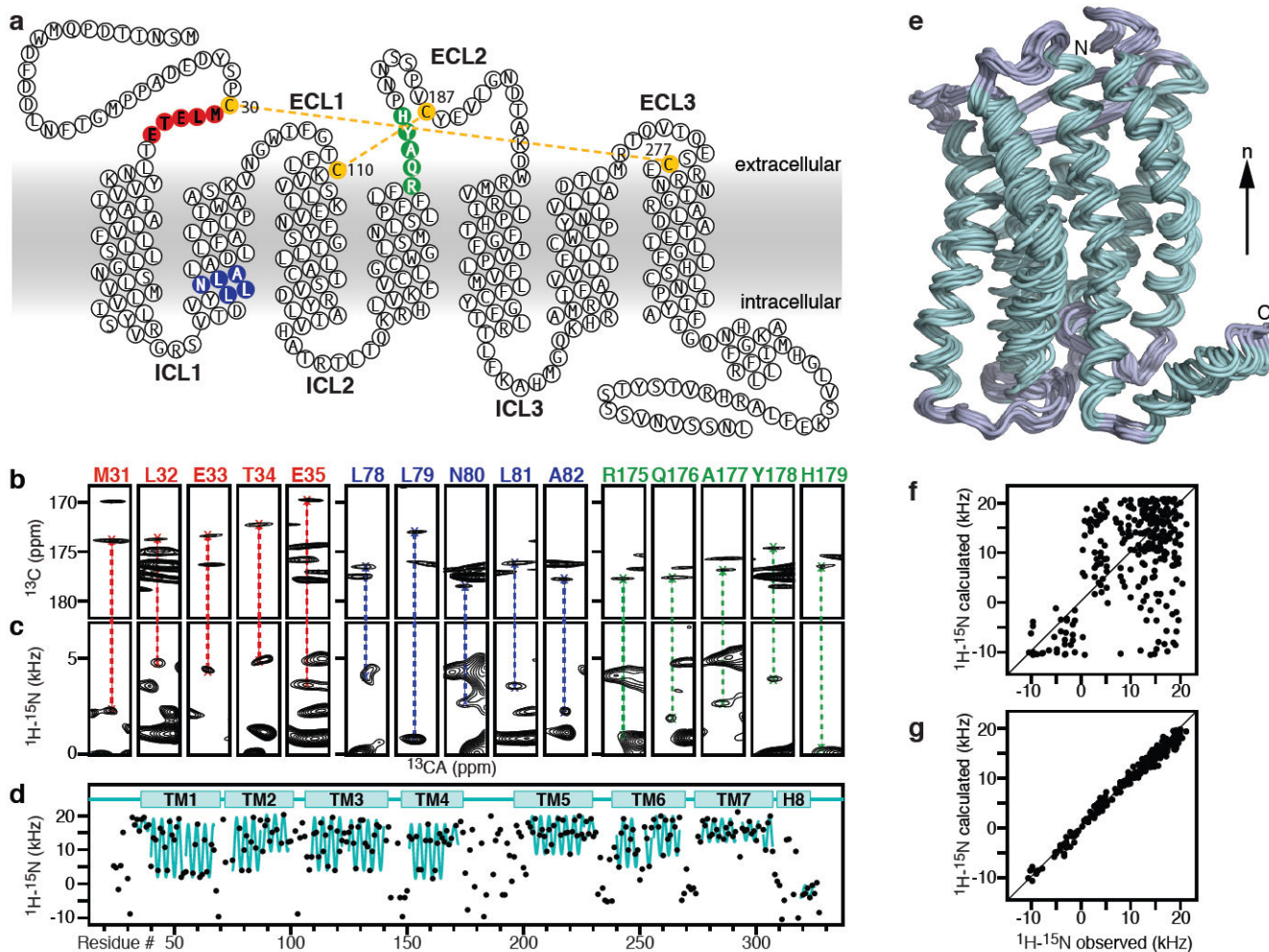
Figure 1. Structure determination of CXCR1

a, CXCR1 topology with four disulfide bonds (gold). **b-c**, Strip plots from three-dimensional experiments taken at specific ^{15}N and ^{13}CA chemical shifts for three representative regions of CXCR1: N-terminus (residues 31-35) (red), TM2 (residues 78-82) (blue), and ECL2 (residues 175-179) (green). **b**, NCACX data used for resonance assignments. **c**, ^{13}C-detected ^{1}H-^{15}N SLF spectra. **d**, Dipolar wave plot of the experimentally measured ^{1}H-^{15}N DC values as a function of residue number. Sinusoidal fits (cyan) to the data (4.1 kHz RMSD) highlight the transmembrane (TM1-TM7) and C-terminal (H8) helices. **e**, Ensemble of 10 lowest energy structures of CXCR1 aligned in the membrane (n: bilayer normal). **f-g**, Correlation plots of experimental and back-calculated ^{1}H-^{15}N DC restraints obtained (**f**) before and (**g**) after refinement against the experimental data.
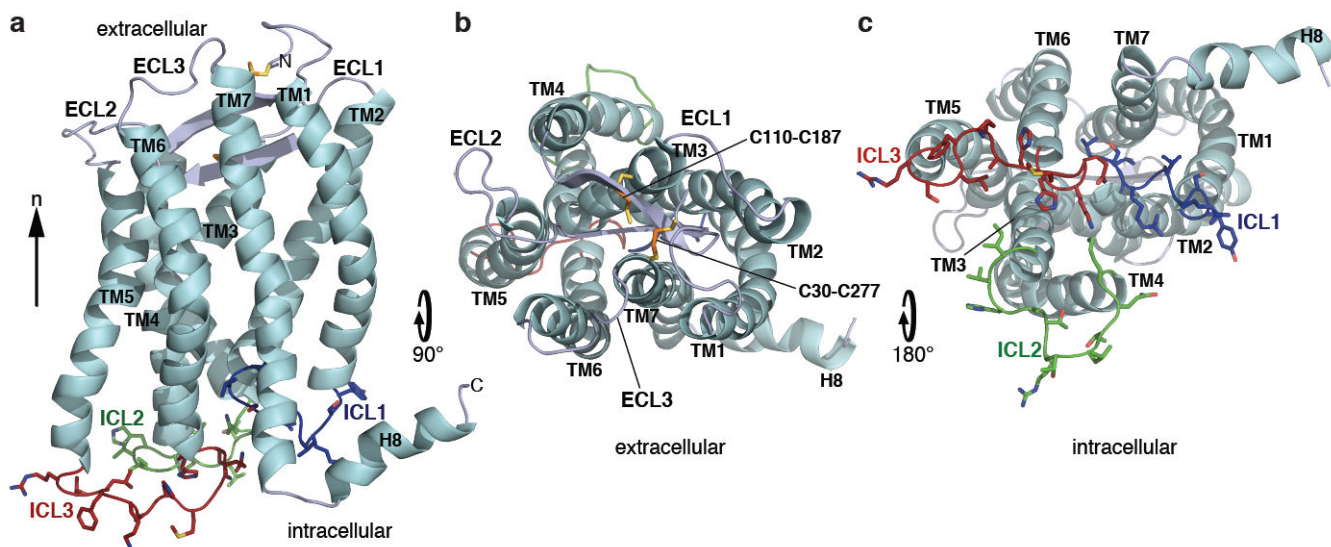
Figure 2. Three-dimensional structure of CXCR1
Backbone representation of CXCR1 showing helices (TM1-TM7 and H8) in aqua,
extracellular loops (ECL1-ECL3) in gray, and intracellular loops in blue (ICL1), green
(ICL2) and red (ICL3). Disulfide bonded Cys pairs (C30-C277; C110-C187) are shown as
sticks. **a**, Side view (n: bilayer normal). **b**, View from the extracellular side. **c**, View from
the intracellular side.
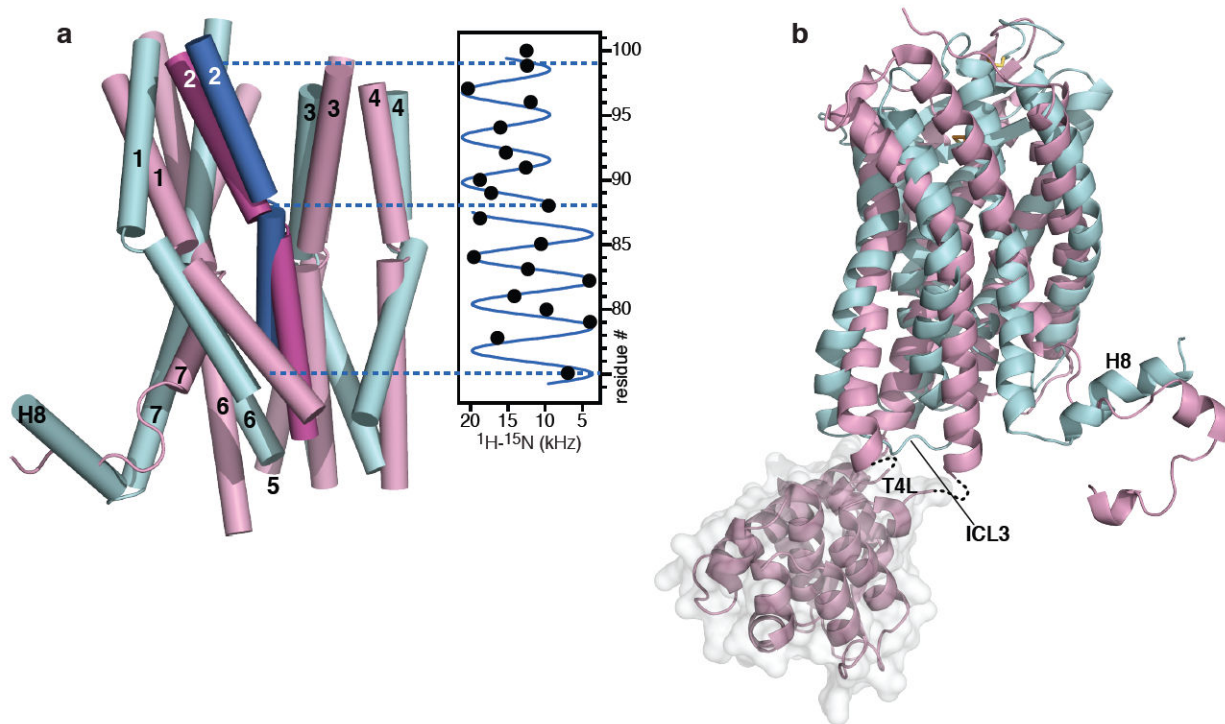
Figure 3. Structural comparison of CXCR1 (cyan, PDB ID: 2LNL) and CXCR4 (pink, PDB ID: 3ODU)

a, Comparison of TM helices. TM2 (residues 74-101) of CXCR1 (blue) has a kink that changes helix direction at Phe88. The kink is reflected in disruption of the dipolar wave near Phe88. TM2 of CXCR4 (magenta) has a kink at the same location (Phe87). **b**, Comparison of backbone structures. The third intracellular loop (ICL3) of CXCR4 is replaced by T4 lysozyme (T4L, molecular surface representation). The C-terminus of CXCR1 forms a well-defined amphipathic helix (H8), while that of CXCR4 is only loosely helical.